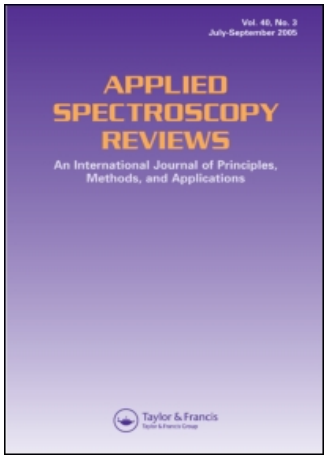

Applied Spectroscopy Reviews
Publication details, including instructions for authors and subscription information:
http://www.informaworld.com/smpp/title~content=t713597229

Photoacoustic Gas Analysis Using Interferometric Cantilever Microphone

Tom Kuusela [a]; Jyrki Kauppinen [a]
[a] Department of Physics, University of Turku, Turku, Finland

Online Publication Date: 01 September 2007
To cite this Article: Kuusela, Tom and Kauppinen, Jyrki (2007) 'Photoacoustic Gas Analysis Using Interferometric Cantilever Microphone', Applied Spectroscopy Reviews, 42:5, 443 - 474
To link to this article: DOI: 10.1080/00102200701421755
URL: http://dx.doi.org/10.1080/00102200701421755

Applied Spectroscopy Reviews, 42: 443–474, 2007

ISSN 0570-4928 print/1520-569X online
DOI: 10.1080/00102200701421755

Taylor & Francis
Taylor & Francis Group

Photoacoustic Gas Analysis Using Interferometric Cantilever Microphone

Tom Kuusela and Jyrki Kauppinen
Department of Physics, University of Turku, Turku, Finland

Abstract: Theoretical considerations and a simple but realistic model of the function of the cantilever-based photoacoustic trace gas system are presented. The essential features of the cantilever dynamics, thermal characteristics, and noise models are derived. Some other related constructions are shown with the practical implementations of the real system.

Keywords: Gas analysis, trace gas, photoacoustic, cantilever, interferometer, FTIR

INTRODUCTION

The photoacoustic effect is the process of acoustic wave generation in the sample resulting from the absorption of photons. This process was invented already at the end of the 1800s (1, 2) but first real applications were not introduced until the 1960s (3, 4). The photoacoustic method has since been used to study various chemical and physical phenomena in number of fields. Some of the applications are trace gas analysis, spectroscopy of weak optical transitions, and probing of an optically thick sample. To date, photoacoustic spectroscopy is widely used in many areas of research and applications.

The basic theory behind photoacoustic detection is rather simple (5). Light absorbed in a sample will excite a small fraction of the ground state molecular population to higher energy levels. These excited states will subsequently relax through a combination of radiative and nonradiative pathways. The nonradiative part of the excitations will finally generate heat in the localized region of the light beam and produce a pressure wave,

Received 20 April 2007, Accepted 24 April 2007
Address correspondence to Tom Kuusela, Department of Physics, University of Turku, Vesilinnantie 5, 20014 Turku, Finland. E-mail: kuusela@utu.fi

which propagates away from the source. This pressure wave can be then detected with a suitable sensor such as a microphone. Photoacoustic detection is a unique method since it is a direct monitor of the nonradiative relaxation channel and thus it complements spectroscopic techniques based on absorption and fluorescence. The photoacoustic method is also an extremely sensitive technique, with the ability to detect highly forbidden optical transitions and trace components in a mixture of gases.

In this study we describe the key features and the theoretical backgrounds of the photoacoustic trace gas system when using the cantilever microphone as a pressure sensor.

PHOTOACOUSTIC DETECTION SYSTEM

The essential components of the apparatus used for photoacoustic gas analysis or spectroscopy are a source of modulated light, a sample cell, a sensor for detecting the acoustic signals, and the signal processing system.

Radiation Sources

The light source of the photoacoustic detection system is either a broadband IR source, a continuous wave, or a pulsed laser. When using an IR source, the radiation must be fed to the sample cell through a narrow band-pass filter or monochromator. With a conventional lamp it is very simple to generate lot of infrared power, but the modulation of the infrared source is clumsy; in practice, the only method is to use a mechanical chopper, although low-power semiconductor infrared emitters, which can be modulated by current, are already available. With lasers, the amplitude and frequency modulation is easily performed. However, the suitable wavelengths needed for molecular excitations can be difficult to realize when using laser sources.

Sample Cell Structures

The sample cell design depends on the type of the light source but the main target is always to generate acoustic waves and couple the sensor to acoustic excitations as efficiently as possible. All sample cells can be used either in the nonresonant or resonant mode of operation. If the modulation frequency is much lower than the lowest acoustical resonance frequency, the cell is operated in a nonresonant mode. In this case, the sound wavelength is much larger than the cell dimensions; thus, sound cannot propagate and standing waves cannot form, and the average pressure in the cavity will oscillate with the modulation frequency.

For resonant operation, the modulation frequency is tuned to one of the eigenresonances of the photoacoustic cell. If the eigenresonances are well separated and the Q factor of the particular resonance to be used is large enough, the selected resonance can be excited much more effectively than the others. The set of resonance modes depends on the basic structure of the cell. Three types of acoustic resonators have found widespread use in photoacoustic detection: Helmholz resonators, one-dimensional cylindrical resonators, and cavity resonators (6).

The simplest Helmholz resonator consists of a cavity and an adjoining neck, which opens to open air. When an air plug in the neck moves outward, the pressure inside the cavity decreases, resulting in an inward-directed force, which tries to restore the original state. An oscillation will develop with the resonance frequency depending on the cross-sectional area and the length of the neck and volume of the cavity. The amplification at the resonance frequency depends on the viscous and thermal losses at the wall of the neck and the radiation losses through the opening; in practice, it does not exceed a value of 10. Since a Helmholz resonator cell has to be isolated against outside noise, a simple cavity with a neck is not useful. Therefore, the simplest practical applicable cell consists of two cavities connected by a tube.

If the cross-sectional dimensions of a resonator are much smaller than the acoustic wavelength, the excited sound filed develops a spatial variation only along the length of the resonator. A narrow pipe or tube can be regarded as a one-dimensional acoustic resonator. A pressure wave propagating in the pipe will be reflected by open or closed end with opposite or same phase, and through multiple reflections a standing wave will be formed corresponding to the resonance situation. Pipe resonators are widely used in gas-phase photoacoustics.

If the dimensions of a cavity are comparable with the acoustic wavelength, then several distinct resonances can be generated. The standing wave patterns and resonance frequencies depend strongly on the shape and size of the cavity. Typical resonator constructions are cylinders and spheres where various radial or spherical resonances are possible. Cylindrical cavities are used with laser light sources.

Acoustic Sensors

The device coupling to the acoustic field and converting pressure changes to voltage signal is the most critical part of the apparatus when looking for the best sensitivity in trace gas analysis. Microphones normally used in photoacoustic applications can be divided into two main categories: capacitive and optical. Capacitive microphones are either condenser or electret microphones. Optical sensors are based on measuring the movements of either elastic membrane or silicon cantilever using optical beam deflection method

or an interferometer. Besides these methods it is possible to accumulate the absorbed energy not in the gas but in piezoelectric quartz crystals.

A condenser microphone produces an electrical signal when a pressure wave impinging on the diaphragm pushes the diaphragm closer to the fixed metal plate, thereby increasing the capacitance between the surfaces. The capacitance change leads to a voltage signal, which increases with the bias voltage and diaphragm area. Condenser microphones generally have very flat frequency response and low distortion and respond well to pressure impulses. The dielectric material between the condenser plates in this type of microphone is air. The electret microphone works on the same principle except that the bias voltage for the capacitor is provided by an electret, a thin sheet of material with a permanent electric polarization; thus, no external bias voltage is needed. Due to large capacitance per unit area possible from electret materials, these microphones can be very small.

Both condenser and electret microphones have some fundamental limitations that cannot be overcome (7–9). First, to increase the sensitivity of the microphone, the gap between the elastic membrane and the backplate cannot be decreased below certain limit. If the gap is very narrow, the gas between the membrane and plate cannot flow freely because of viscous effects; therefore, membrane movements are restricted. Secondly, the tension of the membrane cannot decrease too much: if the membrane is very flexible, the dynamic range of the sensor is extremely small. Increasing of the membrane area also cannot improve the function of these microphones since the larger area corresponds to larger movements of the membrane and thus also larger volume changes in the closed sample cell where the microphone is attached. This volume change decreases the magnitude of the pressure pulses and no net increase in the sensitivity can be achieved. The response of the membrane on the external pressure is also nonlinear due to the fact that the material has to stretch out radially under pressure variations. Finally, the output impedance of condenser and electret microphones is very high, especially at low frequencies, necessitating the use of a very high input impedance amplifier for further signal processing. In practice, the noise of the best available amplifiers usually exceeds the noise generated from the transducer itself. Noise features can be improved by using higher modulation frequencies since the noise sources, both intrinsic of the microphone and external acoustic noise, show a characteristic $1/f$ frequency dependence. Unfortunately, the photoacoustic signal is also inversely proportional to the modulation frequency, and thus the signal-to-noise ratio of the gas microphone cell is usually quite low. With resonator cell designs, like the Helmholz resonator, signal-to-noise ratio can be significantly enhanced but then the cell structure is more complicated.

The movement of the elastic membrane can be also measured optically using either an optical beam deflection method (10) or an interferometric technique (11). These methods eliminate the need for electronic detection of the small capacitance changes in the condenser or electret microphone.

In the optical beam approach, the beam of the He-Ne laser is focused either on the reflecting diaphragm or pellicle mounted on the photoacoustic cell. The pressure waves distort the surface of the diaphragm so that the intensity of the reflected beam varies with the modulation frequency of the excitation radiation. This variation is measured with an iris-photodiode or split-photodiode assembly or position-sensing detector. In the interferometric method, the reflecting diaphragm serves as one element of the Michelson or Fabry-Perot type of interferometer. Pressure changes in the interferometer cavity alter the spacing between mirrors, causing a shift in interference fringe patterns, which are then detected with a photodiode. Although the optical detection methods are totally different than condenser microphone solutions, they have shown a sensitivity close to that of conventional microphones. The noise in these optical microphones arises from several sources. The most obvious sources are dark current in the photodiode and shot noise from the laser. Also, fluctuations in the laser frequency, mode hoppings, and variations in the interferometer spacing can have their own contribution in the total noise, although they obviously are not major sources. The diaphragm itself has its own mechanical limitations regardless of the diaphragm movement detection method as described previously.

A cantilever does not have the same mechanical restrictions as a membrane when using it for pressure wave detection in photoacoustic applications (7, 8). A cantilever has two main benefits. First, the string constant of the vibrating cantilever can be quite easily 2 or 3 decades smaller than one of the membrane, and it can be very easily adjusted by changing the dimensions of the cantilever. Secondly, the dynamical range of the cantilever is very large compared to the one of the membrane; i.e., the cantilever can bend even tens of micrometers without any nonlinear or restricting effects. The bending can be measured either using an optical beam or interferometer. If a large dynamical range is needed, the optical beam method is not applicable but the interferometer should be used. The interferometric measuring has an inherently infinite range of dynamics since the bending can be determined over as many wavelengths of the laser as needed. This large dynamic range is directly related to the concentration range of the trace gas that can be measured, an important feature of any gas detection and measure system.

When using a resonator cell, the absorbed energy is accumulated in the acoustic mode of the resonator; i.e., in the gas. The absorbed power and the measured signal are directly proportional to the quality factor of the resonator. Because of intrinsic losses related to gas viscosity and other relaxation processes, the quality factor is clearly less than 100. Another option is to absorb the energy in the sensitive element or sensor itself. Much higher quality factor can be achieved if the absorbing element is piezoelectric quartz crystal (12, 13). The inexpensive quartz tuning fork found on every digital watch (resonance frequency 32,768 Hz) has a quality factor of 20,000 in a vacuum and 8,000 in atmospheric pressure, much higher than in any resonator gas cell. The most important feature of the quartz resonator is its immunity to

background acoustic noise. In general, the ambient acoustic noise is low above 10 kHz since the noise density follows a $1/f$ frequency dependence. At these frequencies, the acoustic wavelength in air is about 1 cm or longer at lower frequencies. Since the distance of the two prongs of the quartz tuning fork is less than 1 mm, the sound waves from a distant source tend to apply a force in the same direction upon the prongs, and no piezoelectrically active mode is excited.

Photoacoustic systems based on quartz resonators have a few drawbacks. Since the resonance frequencies of the quartz resonators are moderately high, only lasers can be used as a photoacoustic excitation source; infrared sources based on conventional lamp or other blackbody radiator cannot be modulated with such a high frequency. The modulation frequency has to be controlled very accurately since the width of the resonance is very narrow. Even slight drift in the frequency can erroneously decrease the signal significantly.

THEORY OF THE CANTILEVER OPERATION

The basic construction of the photoacoustic system with an interferometric cantilever microphone is shown in Figure 1 (7, 8). It consists of the photoacoustic cell of the volume V filled with the gas under study, the infrared source, the chopper for light modulation, the optical filter, the cantilever, and the interferometer. The interferometer has been draw schematically; the actual device includes several photodiodes as detectors. The interferometer is close to its own chamber of the volume V_0. The cantilever is attached between the photoacoustic cell and the interferometer chamber.

The structure of the silicon cantilever is presented in Figure 2. A very thin, typically 5–10 μm, cantilever part moves like a flexible door when there is a pressure difference over the cantilever. The frame around the cantilever is thick (300–500 μm), and therefore it forms a rigid supporting

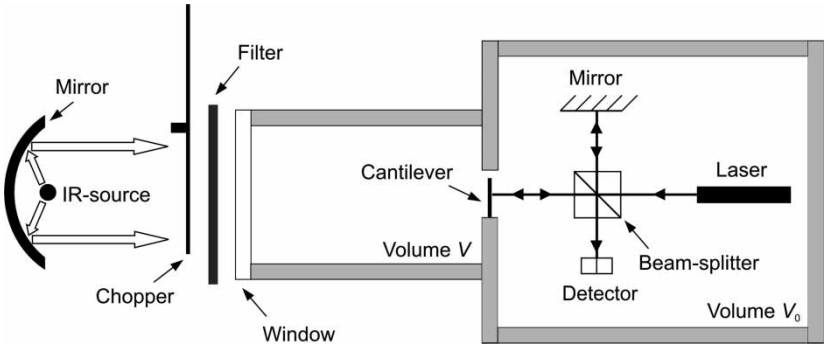

Figure 1. The typical construction of the photoacoustic trace gas detection system using the interferometric cantilever as a microphone.

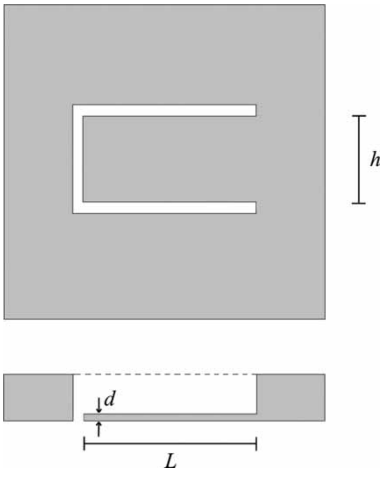

Figure 2. Structure of the silicon cantilever and its frame.

structure. There is a narrow gap (5–30 μm) between the frame and the cantilever on three sides. The length and width of the cantilever are a few millimeters. When the pressure in the surrounding gas varies, the cantilever bends but it does not stretch. Therefore, it is very sensitive to pressure variations compared to the stretching of the elastic membrane.

Cantilever Dynamics

The cantilever can vibrate in several different modes. However, if we are only interested in the frequency region below the first resonance frequency, the full three-dimensional structure model can be replaced with a simple one-dimensional point of mass model in the form of a harmonic oscillator. Therefore, the equation of motion is

$$m\ddot{x} + D\dot{x} + kx = F_{ext}(t) \tag{1}$$

where m is the effective mass, D is the damping factor, and k is the effective spring constant of the cantilever. $F_{\text{ext}}(t)$ is an external force acting on the cantilever. The displacement x from the equilibrium is defined at the free end of the cantilever. As will be shown later, both the mass and the spring constant are not solely determined by the structure of the cantilever in this model but they also depend on the environment; i.e., the features of the photoacoustic cell. The spring constant of the cantilever alone is

$$k_0 = \frac{2}{3}hE\left(\frac{d}{L}\right)^3 \tag{2}$$

where h is the width, L the length, and d the thickness of the cantilever, and E is the Young's modulus of the material (14).

If the external force in Eq. (1) is a simple sinusoid as $F_{\text{ext}}(t) = F_0 \cos(\omega t + \phi)$, the displacement $x(t)$ can be easily solved. The amplitude of the sinusoidal oscillation of $x(t)$ or frequency response is then

$$A(\omega) = \frac{F_0}{m\sqrt{(\omega_0^2 - \omega^2)^2 + (\omega D/m)^2}} \tag{3}$$

where the resonance frequency is defined as $\omega_0 = \sqrt{k/m}$. The frequency response of the cantilever system based on the result (3) is shown in Figure 3. It has a peak on the resonance frequency. The width and height of the resonance peak depends strongly on the damping factor D. If the frequency range of interest is much lower than the resonance frequency ω_0 (and the damping factor D is not extremely high), the frequency response reduces to a constant value

$$A(\omega) = \frac{F_0}{m\omega_0^2} \tag{4}$$

In contrast, if the frequency is much higher than the resonance frequency, the frequency response has a simple functional form

$$A(\omega) = \frac{F_0}{m\omega^2} \tag{5}$$

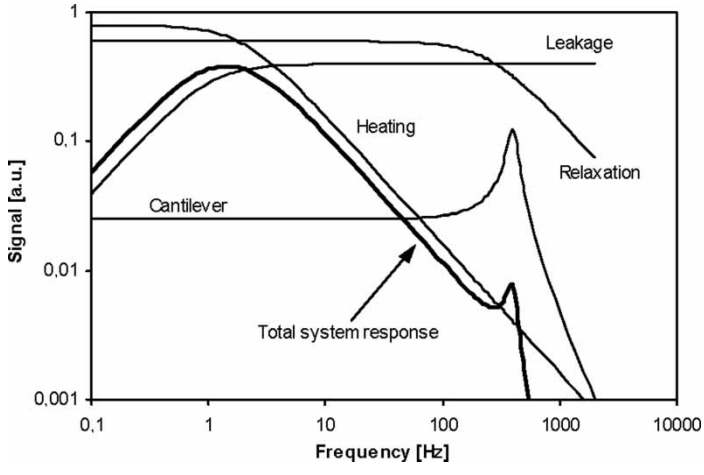

Figure 3. The frequency responses of various mechanisms acting in the photoacoustic system.

Volume Effects of the Photoacoustic Cell

When the effects of the photoacoustic cell on the frequency response of the system is studied, few assumptions can be made. First, if the dimensions of the cell are much smaller than the wavelength of the excited acoustical wave, the pressure, temperature, and density of the gas does not depend on the location inside the gas cell. This simplifies the analysis considerably since it is then not necessary to solve the complicated three-dimensional velocity field of the gas. In this situation we can utilize directly the equation of the state of the ideal gas

$$\frac{dp}{p} + \frac{dV}{V} = \frac{dT}{T} \tag{6}$$

where p is the pressure, V the volume, and T the temperature of the gas in the cell. According to the first law of thermodynamics, the heat energy Q_e going into the gas can be expressed as

$$dQ_e = nC_V \mathrm{d}T + pdV \tag{7}$$

where n is the number of moles and C_V is the molar heat capacity at constant volume. By combining Eqs. (6) and (7) we get

$$\frac{dp}{p} + \kappa\frac{dV}{V} = \frac{(\kappa - 1)dQ_e}{pV} \tag{8}$$

with the help of the relations $\kappa = C_p/C_V$ and $C_p - C_V = R$; R is the universal gas constant. When the pressure change dp affects the cantilever, it produces a displacement dx, which we can get from the force relation

$$k_0 dx = A_c dp \tag{9}$$

where A_c is the area and k_0 the string constant of the cantilever. As the cantilever bends, it introduces a corresponding change on the volume of the photoacoustic cell. If we assume that the cantilever bends in the shape of arc of the circle, the differential volume change is

$$dV = \frac{2}{5}A_c dx \tag{10}$$

Substituting Eqs. (9) and (10) into Eq. (8) we can obtain

$$\left(k_0 + \kappa\frac{A_c^2 p}{2.5V}\right)dx = \frac{A_c(\kappa - 1)dQ_e}{\mathrm{V}} = dF \tag{11}$$

From this result we can deduce some important factors. The right side of Eq. (11) clearly represents a harmonic force, but the spring constant is not the one of the cantilever but has been modified with an additional part, which is originated from the volume change due to bending of the cantilever;

i.e., the cell itself acts like a gas spring. It should be noticed that this part is inversely related to the volume of the cell; thus, if the volume is small, the effect of this part is significant. The result is accurate only under the assumption that the volume of the interferometer chamber (see Figure 1) is large compared to V. The left side of Eq. (11) links the external heating energy Q_e to the above-mentioned harmonic force. Thus, we can write the total force acting on the cantilever by integrating Eq. (11):

$$F_{ext}(t) = \frac{A_c(\kappa - 1)}{V} \int \frac{dQ_e}{dt} dt \tag{12}$$

If we know the power of the heat source inside the sample cell, the term $\mathrm{d}Q_e/\mathrm{d}t$, we can compute the external force from Eq. (12), substitute it to the equation of motion (1), and finally solve the displacement $x(t)$. For the spring constant we should use the modified value

$$k = k_0 + \kappa \frac{A_c^2 p}{2.5V} \tag{13}$$

If the volume of the interferometer chamber V_0 is small, the sample cell volume V in Eqs. (12) and (13) must be replaced with the effective volume V_{eff} determined from the relation

$$\frac{1}{V_{eff}} = \frac{1}{V} + \frac{1}{V_0} \tag{14}$$

This corresponds to the situation where there are two serial-coupled air springs with the moving piston between them.

Heating of the Sample Gas

A photoacoustic signal is generated by the absorption of energy from the modulated light beam. This absorbed energy produces a periodically varying heat source that acts as a source of pressure waves. Without any heat leaks, the temperature of the gas in the cell will increase monotonically. However, there are various mechanisms that carry energy away from the gas. The first one is the thermal conduction through the gas to the walls of the cell and further to the surroundings. As the thermal conduction of the metal walls of the cell is much higher than thermal conduction through the gas, the latter is, in practice, the limiting factor unless the sample cell is very small. We can also assume that the heat capacity of the cell structure is much higher than the heat capacity of the gas; thus, the cell wall can sink a considerable amount of energy without any increase in temperature. Under these assumptions, the heat energy rate is given by the equation

$$\frac{dQ_e}{dt} = \alpha_x p_x l P_0 [1 - \cos(\omega t)] - G(T - T_0) \tag{15}$$

where α_x is the absorption coefficient, p_x the partial pressure of the absorbing gas, l the length of the sample cell, P_0 the maximum power of the light beam, G the total thermal conductivity of the gas content inside the cell, T the temperature, and T_0 the initial temperature of the gas. The first term on the right side of Eq. (15) represents the energy source in the form of the light beam modulated by an angular frequency ω, and the last term represents the heat transfer through the gas. We have assumed here that all absorbed energy is transferred to heat energy, but it is possible that a small part of the energy radiates away from the cell. If the sample cell is long, the linear absorption factor $\alpha_x p_x l$ must be replaced with an exponential factor $1 - \exp(-\alpha_x p_x l)$ as stated by the Beer's absorption law. In the case of a typical cantilever-based system, the cell and the light path is always very short.

If we consider an isochoric (isovolumetric) process, $dQ_e = C_V\, dT$, where C_V is the total heat capacity of the gas in the sample cell, we can approximate (more accurate analysis is done later) for the temperature:

$$\frac{dT}{dt} = \frac{\alpha_x p_x l P_0}{C_V}(1 - \cos(\omega t)) - \frac{G}{C_V}(T - T_0) \tag{16}$$

The solution of this first-order differential equation is

$$T(t) = \frac{\alpha_x p_x l P_0}{G^2 + \omega^2}[G\sin(\omega t) - \omega\cos(\omega t)] + \frac{\alpha_x p_x l P_0}{G} + C_0 e^{-G/C_V t} \tag{17}$$

where the constant C_0 is determined from the initial condition $T(0) = T_0$. The last exponential term is a transient that vanishes in time; thus it can be omitted when looking for the steady-state situation. Using Eq. (17) we obtain

$$\begin{aligned}\int \frac{dQ_e}{dt}dt = \int C_V \frac{dT}{dt}dt &= \frac{C_V \alpha_x p_x l P_0}{G^2 + \omega^2}[G\sin(\omega t) - \omega\cos(\omega t)] \\ &= \frac{\alpha_x p_x l P_0 C_V/G}{\sqrt{1 + ((C_V/G)\omega)^2}}\cos(\omega t + \phi')\end{aligned} \tag{18}$$

where ϕ' is a (here unimportant) phase shift. Using Eqs. (3) and (12), we can now construct the (sinusoidal) external force, apply it in the equation of motion (1), and finally compute the frequency response

$$A_1(\omega) = \frac{A_c(\kappa - 1)}{V}\frac{a_x p_x l P_0}{m\sqrt{(\omega_0^2 - \omega^2)^2 + (\omega D/m)^2}}\frac{\tau_1}{\sqrt{1 + (\omega\tau_1)^2}} \tag{19}$$

where the characteristic time constant is $\tau_1 = C_V/G$. The last term acts like a low-pass filter, which damps oscillations above the frequency $1/\tau_1$.

The time constant τ_1 can be estimated when considering a most simple situation where the sample cell is a long cylinder (no significant end effects). We also assume that the heat energy is absorbed homogeneously everywhere inside the sample cell. If the initial and boundary conditions are

independent of the cylindrical coordinates z and θ, the equation of the heat conduction in the cylindrical coordinates reduces to

$$\frac{\partial T}{\partial t} = \frac{K}{\rho c_v}\left(\frac{\partial^2 T}{\partial r^2} + \frac{1}{r}\frac{\partial T}{\partial r}\right) \tag{20}$$

where K is the thermal conductivity, ρ the density, and c_v the specific heat capacity of the gas. To calculate the time evolution of the temperature, we assume that the initial temperature of the gas in the cylinder is T_0 and the wall of the cylinder is maintained in the constant temperature T_w; i.e., $T(R,0) = T_w$, where R is the radius of the cylinder. Under these conditions, Eq. (20) has the solution (see Carslaw and Jaeger (15)):

$$T(r,t) = T_w + 2(T_0 - T_w)\sum_{n=1}^{\infty} \exp(-\alpha_n^2 t/\tau_c)\frac{J_0(\alpha_n r/R)}{\alpha_n J_1(\alpha_n)} \tag{21}$$

where J_0 and J_1 are the Bessel functions, α_n are the real positive roots of equation $J_0(\alpha) = 0$, and

$$\tau_c = \frac{\rho c_v}{K}R^2 \tag{22}$$

The average temperature of the cylinder is found to be

$$T_{av}(t) = \frac{2}{R^2}\int_0^R rT(r,t)dr = T_w + 4(T_0 - T_w)\sum_{n=1}^{\infty}\frac{1}{\alpha_n^2}\exp(-\alpha_n^2 t/\tau_c) \tag{23}$$

From these results we can see that the time evolution of the temperature is not simple exponential but it has several exponentially decreasing terms. In fact, we have assumed exponential time evolution in the Eq. (16), which is, however, a rather good approximation since the series (23) converges quite rapidly, and the first term is dominant. The corresponding time scale of this term is

$$\tau_{c1} = \frac{\tau_c}{\alpha_1^2} = \frac{\tau_c}{5.78} \tag{24}$$

In the first-order approximation we can use the time constant (24) in the frequency response (19).

Effects of the Cantilever Frame Gap

Since there is a narrow gap between the cantilever and frame, the gas leaks from the photoacoustic sample cell to the other cell containing the interferometer. This leak directly damps the pressure variations but also affects the temperature increase in the sample cell due to the light absorption since the hot gas molecules transfer energy away from the sample cell even if there is no

pressure difference between the cells. Both mechanisms have their own contribution to the frequency response of the system. In the next we sections, we study these mechanisms separately.

Gas Flow Due to Pressure Difference

The gas leak between the cells can be solved using the simple kinetic-molecular model of an ideal gas. Let us assume that the volume of the sample cell is V, pressure p, temperature T_0, and the number of gas molecules N, and in the interferometer chamber V_0, p_0, T_0, and N_0, respectively. Thus we have assumed the temperature is equal in both cells. The total area of the gap between the cantilever and the frame is A_g.

The next step is to compute the number of molecules colliding or passing the area A_g. To begin, we assume that all molecules in the gas have the same magnitude of velocity $|v_x|$ in the direction of the normal to the area A_g. Then the number of molecules that collide with A_g during the small time interval dt is equal to the number of molecules within a cylinder with base area A_g and length $|v_x|\ dt$. The volume of such a cylinder is $A_g|v_x|\ dt$. If the number of molecules per unit volume (N/V) is uniform, the number of molecules in this cylinder is $(N/V)\ A_g|v_x|\ dt$. On average, half of these molecules are moving toward A_g and half are moving away, so the final number of molecules going through the area A_g is $(1/2)\ (N/V)\ A_g|v_x|\ dt$.

The net decrease of the number of molecules in the sample cell is now

$$-dN = \frac{1}{2}\left(\frac{N}{V}\right)A_g|v_x|dt - \frac{1}{2}\left(\frac{N_0}{V_0}\right)A_g|v_x|dt \tag{25}$$

where the last term represents the molecules coming from the interferometer chamber. Since the total number of molecules cannot change, $dN_0 = -dN$. For the system of all molecules in the gas, the total momentum change dP_x during dt is the number of passing molecules multiplied by $2m|v_x|$. The rate of change of momentum is then

$$\frac{dP_x}{dt} = \frac{NA_g m v_x^2}{V} \tag{26}$$

But the rate of change of momentum equals the force exerted on the area A_g by the gas molecules; thus, the force per unit area is the pressure

$$p = \frac{Nmv_x^2}{V} \quad \text{and} \quad p_0 = \frac{N_0 m v_x^2}{V_0} \tag{27}$$

By solving N and N_0 from Eqs. (27) and substituting them into Eq. (25) we obtain

$$-dp = \frac{1}{2}A_g|v_x|\left(\frac{p}{V} - \frac{p_0}{V}\right)dt + dp_{ext} \tag{28}$$

where we have added the external (time-dependent) pressure term sourced by the light absorption in the sample cell. The corresponding equation for p_0 is (without any external pressure source)

$$dp_0 = \frac{1}{2}A_g|v_x|\left(\frac{p}{V_0} - \frac{p_0}{V_0}\right)dt \tag{29}$$

In practice, only the pressure difference between the sample cell and the interferometer chamber is important. If we define $p_d = p - p_0$ we finally get

$$\frac{dp_d}{dt} + \frac{1}{2}A_g|v_x|\frac{1}{V_{eff}}p_d = \frac{dp_{ext}}{dt} \tag{30}$$

where the effective volume is determined previously in Eq. (14). This first-order differential equation can be easily solved. If we omit the exponential transient solution of the homogenous equation and assume that the external pressure is sinusoidal, i.e., $p_{\text{ext}}(t) = G_0 \sin(\omega t)$, the solution of Eq. (30) is

$$p_d(t) = \frac{G_0\omega\tau_2}{\sqrt{1+(\omega\tau_2)^2}}\cos(\omega t + \phi'') \tag{31}$$

where the characteristic time constant is

$$\frac{1}{\tau_2} = \frac{1}{2}A_g|v_x|\frac{1}{V_{eff}} \tag{32}$$

In reality $|v_x|$ or v_x^2 is not the same for all molecules. However, we can replace v_x^2 with average value $(v_x^2)_{av}$. Since there is no real difference between x-, y-, and z-directions in the ideal gas model, we can write $(v_x^2)_{av} = 1/3(v^2)_{av}$. Now Eq. (27) becomes $pV = 2/3\ N[1/2m(v^2)_{av}]$. Using the ideal gas equation $pV = nRT_0$, we can first obtain the average translational kinetic energy of a gas molecule $1/2m(v^2)_{av} = 3/2k_BT_0$, where k_B is the Boltzmann constant and T is the temperature, and finally the root mean square speed of a gas molecule of a mass m

$$v_{rms0} = \sqrt{(v^2)_{av}} = \sqrt{\frac{3k_BT_0}{m}} \tag{33}$$

which can be used in Eq. (32) to replace $|v_x|$. Now we can write the frequency response of the leakage of the gap:

$$A_2(\omega) = \frac{G_0\omega\tau_2}{\sqrt{1+(\omega\tau_2)^2}} \tag{34}$$

This corresponds to a high-pass filter since $A_2(\omega) \approx 0$ when $\omega \approx 0$, and $A_2(\omega) \rightarrow$ constant G_0 when $\omega \gg \tau_2$. Frequencies below $1/\tau_2$ are strongly damped.

Energy Transfer Due to Temperature Difference

Also in this case we can use a simple kinetic model of an ideal gas. We assume now that the volume of the sample cell is V, pressure p, temperature T, and the number of gas molecules N, and in the interferometer chamber V_0, p, T_0, and N_0, respectively. Thus, we have assumed that the pressure is equal in both cells. Since the temperature inside the cells is not equal, the mean velocities of the molecules are different, here v_x and v_{x0}. This velocity difference produces net gas flow through the gap between the cantilever and the frame.

The internal energy of the gas in the cell is the number of molecules passing through the area A_g multiplied by the kinetic energy of one molecule $1/2mv_x^2$. The net change of the internal energy U of the sample cell is

$$-dU = \frac{1}{2}\left(\frac{N}{V}\right)A_g v_x dt\left(\frac{1}{2}mv_x^2\right) - \frac{1}{2}\left(\frac{N_0}{V_0}\right)A_g v_{x0} dt\left(\frac{1}{2}mv_{x0}^2\right) \tag{35}$$

The last term is the contribution of the molecules coming from the interferometer chamber. As shown in the previous case, the average kinetic energy of a gas molecule is equal to $3/2k_BT$, so for N molecules we can write the internal energy

$$dU = \frac{3}{2}k_B N dT \tag{36}$$

Since the pressure is equal in both cells, $N_0/V_0 \approx N/V$. By combining Eqs. (35) and (36), replacing v_x and v_{x0} with the root mean square speeds v_{rms} and v_{rms0} ($(v_x^2)_{av} = 1/3(v^2)_{av} = 1/3v_{rms}^2$), and adding the external time-dependent temperature source T_{ext}, we obtain

$$dT = -\frac{mA_g}{6k_B V}\left(\frac{1}{3}\right)^{3/2}(v_{rms}^3 - v_{rms0}^3)\,dt + dT_{ext} \tag{37}$$

Further, we can use the Eq. (33) to convert root mean square speeds to temperatures in order to get the differential equation for temperature:

$$\frac{dT}{dt} = -\frac{A_g}{6V}\sqrt{\frac{k_B}{m}}\left[T^{3/2} - T_0^{3/2}\right] + \frac{dT_{ext}}{dt} \tag{38}$$

Since this equation is nonlinear, its solution cannot be found analytically. However, since we are only interested in the temperature difference between the cells, we can write $T = T_0 + T_d$, where T_d is very small, and approximate

$$T^{3/2} = \left[T_0\left(1 + \frac{T_d}{T_0}\right)\right]^{3/2} \approx T_0^{3/2}\left(1 + \frac{3}{2}\frac{T_d}{T_0}\right) \tag{39}$$

Now the equation for T_d is

$$\frac{dT_d}{dt} = -\frac{A_g}{4V}\sqrt{\frac{k_B T_0}{m}}T_d + \frac{dT_{ext}}{dt} \tag{40}$$

If we omit the exponential transient solution of the homogenous equation, as we did in the previous case, and assume that the external temperature source is sinusoidal, i.e., $T_{ext}(t) = H_0 \sin(\omega t)$, the solution of Eq. (40) is

$$T_d(t) = \frac{H_0 \omega \tau_3}{\sqrt{1 + (\omega\tau_3)^2}}\cos(\omega t + \phi''') \tag{41}$$

where the characteristic time constant is

$$\frac{1}{\tau_3} = \frac{A_g}{4\sqrt{3}V}\sqrt{\frac{3k_B T_0}{m}} = \frac{A_g}{4\sqrt{3}V}v_{rms0} \tag{42}$$

and the corresponding frequency response

$$A_3(\omega) = \frac{H_0 \omega \tau_3}{\sqrt{1 + (\omega\tau_3)^2}} \tag{43}$$

It should be noted that the functional form of the frequency response (43) is equal to the one of Eq. (34). In Eqs. (35) and (36) we have assumed that the internal energy of the interferometer chamber is constant. If more precise analysis is done (not shown here), the only modification in our first-order approximation is that the sample cell volume V in Eq. (42) should be replaced with the effective volume V_{eff}.

If we compare the characteristic time scales (32) and (42), we find that they are very similar; the only difference is the factor of 2. Although the two processes, gas flow due to pressure difference and temperature difference, have been treated separately, the total mechanism can be regarded as a serial mechanism of these two processes. Then the effective time constant is

$$\frac{1}{\tau_{23}} = \frac{1}{\tau_2} + \frac{1}{\tau_3} = \frac{3}{2}\frac{A_g}{4\sqrt{3}V_{eff}}v_{rms0} = \frac{3A_g}{4\sqrt{\kappa}V_{eff}}v_{sound} \tag{44}$$

where we have replace the root mean square molecular velocity with the sound velocity in the gas ($v_{rms0} = \sqrt{3/\kappa}v_{sound}$). As long as the gas flow through the gap between the cantilever and the frame is low enough, the above-described analysis is valid. If the flow increases, there is a limit for gas flow; namely, the sound velocity. After that limit, the flow does not depend on the pressure (or temperature) difference.

Relaxation Mechanism from Light Absorption to Heat

When light enters to the sample cell, it will excite a small fraction of the molecules in the ground state to higher energy levels. These excited states will relax through both radiative and nonradiative pathways, but only the nonradiative part of the excitations will generate heat. The pathways can be very complex and the contribution of each path could be very difficult to estimate. The relaxation time from the absorption to heat generation depends on the complexity of the pathway and the energy levels of the excited states. However, the total relaxation process can be modeled using one effective relaxation time constant. The process acts like a low-pass filter whose frequency response is

$$A_4(\omega) = \frac{J_0}{\sqrt{1 + (\omega\tau_4)^2}} \tag{45}$$

where τ_4 is the effective relaxation time constant. Typically the relaxation time is less than 1 ms and therefore it is not important if the operation frequency is well below the characteristic frequency $1/\tau_4$, as it is in cantilever-based systems. However, in the cell configurations utilizing resonances on the frequency range of kilohertz and especially in quartz-enhanced photoacoustic devices, where the modulation frequency is typically tens of kilohertz, relaxation processes significantly reduces the sensitivity, and the responsitivity depends strongly on the gas mixture.

The frequency response of the complete system is the product of the responses of each separate mechanism and process described in Eqs. (19), (34), (43), and (45). The two responses can be combined with the help of Eq. (44). Thus, we obtain the total frequency response (the frequency responses (34), (43), and (45) must be divided by G_0, H_0, and J_0 in order to obtain transfer functions):

$$A_{tot}(\omega) = \frac{A_c(\kappa - 1)}{V} \frac{a_x p_x l P_0}{m\sqrt{(\omega_0^2 - \omega^2)^2 + (\omega D/m)^2}} \frac{\tau_1}{\sqrt{1 + (\omega\tau_1)^2}} \frac{\omega\tau_{23}}{\sqrt{1 + (\omega\tau_{23})^2}} \frac{1}{\sqrt{1 + (\omega\tau_4)^2}} \tag{46}$$

The contribution of each response is shown in Figure 3. The cantilever itself has flat frequency response until the resonance frequency, where it has a sharp peak. On lower frequencies, the gas leakage through the gap between the cantilever and the frame strongly decreases the sensitivity of the system. The heating mechanism of the sample gas drops the sensitivity at the higher frequencies. As a combination of all mechanisms, the total system typically has a wide maximum in the frequency range of 1–10 Hz. Experiments with various sample cells have demonstrated that observed frequency responses can be well fitted to Eq. (46).

NOISE CHARACTERISTICS

The sensitivity of the trace gas detection system is a most important parameter, but high responsivity itself does not guarantee that the system is really useful for measuring small gas concentrations. As important factor is the noise level or signal-to-noise ratio (SNR). There are four noise sources of the cantilever-based photoacoustic systems: acceleration noise, acoustical noise, Brownian noise, and electrical noise.

Acceleration Noise

The acceleration noise is generated from the movements of the cantilever because of the external disturbances acting on the system. Typically these disturbances are low-frequency vibrations of the environment that couple directly to the support structure of the device and thereby to the cantilever. Only such acceleration components that are perpendicular to the surface of the cantilever can make the cantilever bend and produce noise. The signal-to-noise ratio can be determined as

$$SNR(\omega) = \frac{A_{tot}(\omega)}{\text{Noise amplitude}}. \tag{47}$$

In the case of external vibration affecting the cantilever we can write

$$\Delta F = m\Delta a = \rho_c A_c d\Delta a = k\Delta x, \tag{48}$$

where the m_{cant} is the mass of the cantilever, Δa is the amplitude of the acceleration noise, Δx the corresponding movement, and ρ_c the material density of the cantilever. If $\omega\tau_1 \gg 1$, $\omega\tau_{23} \gg 1$, and $\omega\tau_4 \ll 1$, the frequency response (46) can be simplified. By solving Δx from Eq. (48) and using it as noise amplitude in Eq. (47) we obtain

$$\begin{aligned} SNR_{accel}(\omega) &= \frac{A_c(\kappa-1)\alpha_x p_x l P_0}{V} \frac{1}{\omega m\sqrt{(\omega_0^2-\omega^2)^2+(\omega D/m)^2}} \frac{1}{\rho_c A_c d\Delta a/k} \\ &= \frac{(\kappa-1)\alpha_x p_x l P_0}{\omega(m/k)\sqrt{(\omega_0^2-\omega^2)^2+(\omega D/m)^2}V\rho_c d\Delta a}. \end{aligned} \tag{49}$$

In the limit $\omega \ll \omega_0$, i.e., when we are looking for the frequencies below the resonance of the cantilever, *SNR* is further reduced to ($\omega_0^2 = k/m$)

$$SNR_{accel}(\omega) \approx \frac{(\kappa-1)\alpha_x p_x l P_0}{\omega V \rho_c d\Delta a} \tag{50}$$

It should be noted that the result (50) does not depend on the area or spring constant of the cantilever. The easiest way to increase *SNR* is to decrease

the cell volume V, but a very small cell can produce other problems, like fast cooling of the sample gas lowering the sensitivity.

Acoustical Noise

Acoustical noise can be generated from external acoustical waves, which leak to the sample cell through holes in the construction, but in normal sample cell design this is rather rare situation. In practice, high-frequency mechanical vibrations often produce acoustical noise if the structure of the sample cell or other parts, like tubes and valves connected to it, act like a microphone; i.e., their walls or sealings are so flexible that they can vibrate under sound pressure. As in the previous case, we can write for the noise amplitude

$$\Delta F = A_c \Delta p = k \Delta x \tag{51}$$

where Δp is the amplitude of the acoustical pressure noise, and the corresponding *SNR* is

$$SNR_{acoust}(\omega) = \frac{(\kappa - 1)\alpha_x p_x l P_0}{\omega(m/k)\sqrt{(\omega_0^2 - \omega^2)^2 + (\omega D/m)^2} V \Delta p}$$

$$\approx \frac{(\kappa - 1)\alpha_x p_x l P_0}{\omega V \Delta p} \tag{52}$$

where the last version is the low-frequency limit. This is very similar to the acceleration *SNR* in Eq. (49) or Eq. (50).

Brownian Noise

The cantilever can be regarded as a one-dimensional harmonic oscillator immersed in a viscous medium when the equation of motion can be written as

$$m\ddot{x} + D\dot{x} + kx = F_{ext}(t) + F_{th}(t) \tag{53}$$

where $F_{th}(t)$ is the random force due to thermal fluctuations (16–18). Since the thermal fluctuations are mediated by collisions between the molecules in the medium and the cantilever, the random forces are completely uncorrelated for a time scale much longer than the mean collisions time. The fluctuating force $F_{th}(t)$ comes about because of the randomness of the individual impacts from the molecules that make up the medium responsible for the deterministic friction force $-D\dot{x}$, as proven by the fluctuation-dissipation theorem (19).

In thermodynamic equilibrium, if we assume that force on the cantilever is solely thermal in origin, the expectation value of the potential energy of the cantilever $\langle 1/2kx^2\,(t)\rangle$ is equal to $1/2k_BT$ as long as $\hbar\omega \ll k_BT$. As previously

shown, $x(t)$ in Eq. (53) can be considered to be the output of a linear time-invariant system $H(\omega)$ for an input $F_{th}(t)$ and transfer function

$$H(\omega) = \frac{1}{-m\omega^2 + iD\omega + k} \tag{54}$$

The power spectral density of $x(t)$ is given by

$$S(\omega) = |H(\omega)|^2 S_{th}(\omega) = \frac{1}{(k - m\omega^2)^2 + D^2\omega^2} S_{th}(\omega) \tag{55}$$

where $S_{th}(\omega)$ is the power spectral density of $F_{th}(t)$. Using Eq. (55) we can derive the expectation value of the potential energy in the frequency domain:

$$\begin{aligned} \frac{1}{2}k_B T = \frac{1}{2}k\langle x^2(t)\rangle &= \frac{1}{2}k\frac{1}{2\pi}\int_{-\infty}^{\infty} S(\omega)d\omega \\ &= \frac{1}{4\pi}k\int_{-\infty}^{\infty} \frac{S_{th}(\omega)d\omega}{(k - m\omega^2)^2 + D^2\omega^2} \end{aligned} \tag{56}$$

Assuming that $F_{th}(t)$ is white noise with a spectral density given by a constant σ^2, we obtain, after computing the integral in Eq. (56),

$$\frac{1}{2}k_B T = \frac{k\sigma^2}{4\pi}\frac{\pi}{mD\omega^2} \tag{57}$$

and therefore we have the relation $\sigma^2 = 2k_B TD$. Thus, we have the power spectral density

$$S(\omega) = \frac{2k_B TD}{(k - m\omega^2)^2 + D^2\omega^2} \tag{58}$$

For signal-to-noise ratio we need the root mean square amplitude of the cantilever movement, which is the square root of the power spectral density (whose unit is m^2/Hz) either multiplied with the measurement bandwidth B or divided with the measurement time τ_m. In the low-frequency and small damping limit we obtain

$$\Delta x_{rms} = \sqrt{\langle(\Delta x)^2\rangle} = \sqrt{S(\omega)/\tau_m} = \sqrt{\frac{2k_B TD}{k^2\tau_m}} = \sqrt{\frac{2k_B T}{m\omega_0^3 Q\tau_m}} \tag{59}$$

where the quality Q factor is given by $Q = \omega_0/\Delta\omega = \omega_0 m/D$, where $\Delta\omega$ is the half-width of the resonance peak. The *SNR* with Brownian noise, according to Eq. (47), is

$$SNR_B(\omega) = \frac{A_c(\kappa - 1)\alpha_x p_x l P_0}{\omega V k\sqrt{2k_B T/m\omega_0^3 Q\tau_m}} = \frac{A_c(\kappa - 1)\alpha_x p_x l P_0}{\omega V\sqrt{2k_B Tk/\omega_0 Q\tau_m}} \tag{60}$$

From the result (60), we can see that the SNR_B can be significantly increased either by decreasing the volume V of the sample cell or increasing the Q factor (in practice, decreasing the damping factor D). The Q factor of the

cantilever itself, measured in vacuum conditions, is high, typically several hundreds. When the cantilever is in the gas-filled chamber, the effective Q factor is only 5–10 since the gas flow around the cantilever damps the movements of the cantilever rather efficiently. The Q factor can be artificially increased by introducing external force in Eq. (53), which is directly related to the velocity of the cantilever (20–23). Normally this method has been used to sharpen the resonance peak of the AFM cantilever when the signal amplitude is increased but also the Brownian noise; thus, there is no net effect on the signal-to-noise ratio. In this case, where the operation frequency is well below the resonance, the desired effect is to decrease Brownian noise. Higher Q factor accumulates noise to the resonance peak when the noise on other frequencies decreases since the total Brownian noise integrated over all frequencies is constant.

The signal-to-noise ratio can also be written in the form

$$SNR_B(\omega) = \frac{A_c(\kappa - 1)\alpha_x p_x l P_0}{\omega V \sqrt{2\, k_B T D/\tau_m}} \tag{61}$$

From this form we can realize that actually *SNR* does not depend on the spring constant k; the only parameter directly related to the features of the cantilever is the area A_c. In fact, the damping factor D is the most important parameter when considering *SNR* for Brownian noise. In a free air condition, the damping factor D is directly related to the cantilever area A_c but when the cantilever is operating inside the closed cell the dependence is different. In all cases, however, the damping factor increases when increasing the cantilever area.

We can thus conclude that the spring constant can be easily increased in such a manner that the acceleration, acoustical and especially Brownian noise, if the first ones can be efficiently eliminated, dominates over the electrical noise. For traditional membrane-based microphones, the electrical noise always sets the limits for smallest detectable signal.

Electrical Noise

The electrical noise is originated from various sources on the sensor system. The photodiodes used in the interferometer have their own noise contribution because of the dark current, and the photodiode amplifier some input noise, which can be minimized by using a low-noise version of operational amplifiers. The interferometer laser has mainly shot noise. All these noise sources have different frequency characteristics. In practical implementations of the cantilever-based photoacoustic detection systems, the level of electrical noise is clearly lower than all other noise types. If the external vibrations and acoustical disturbances can be eliminated, Brownian noise is the main noise source.

EXPERIMENTS

The cantilever microphone has been used in various photoacoustic configurations. In most cases, there is no need to optimize the cantilever itself, but the structure and dimensions of the sample cell must be selected to fulfill the special demands of the different applications.

Experiments with Infrared Source

The first experiments using a cantilever microphone were performed with an infrared light source (8). The length of the sample cell was 100 mm and the diameter 10 mm. The IR radiation was fed to the sample cell through bandpass filter with cut-on and cut-off wavelengths of 2.94 and 3.85 μm; methane has a strong absorption band in this range. The resonance frequency of the cantilever inside the sample cell was 470 Hz and the modulation frequency of the infrared source was 118 Hz, accomplished by using a mechanical chopper. The sample cell was filled with a mixture of nitrogen and methane, where concentration of methane was 10 ± 2 ppm, and the total pressure was 0.6 atm. The observed *SNR* was about 1000 with a measurement time of 0.74 s and about 12,000 with a measurement time of 100 s. In the last case, the detection limit was 0.8 ppb. Further, 10 ppm concentration of methane corresponds to 25 nm amplitude of the cantilever, pressure change of 2×10^{-7} Pa, or temperature increase of 2×10^{-9} K. The design of the system was not optimal since, for example, the gap between the frame and the cantilever was rather large, 30 μm, and therefore the cut-off frequency due to gas leakage was approximately 50 Hz. By decreasing the gap, it is possible to decrease the detection limit significantly. These first results already show that cantilever-based photoacoustic method is most promising for trace gas measurements.

Experiments Using Tunable Diode Laser Sources

Tunable DFB (distributed feedback) laser diodes as a light source are potential when constructing compact, selective, highly sensitive, and relatively low-cost trace gas analysis devices. The system configuration with laser sources is quite different when comparing with the photoacoustic detection with traditional IR sources.

First, the laser modulation is accomplished in a different manner. It would be possible to modulate electrically the light intensity by adjusting the laser current but the better method is to modulate the output wavelength of the laser light. In practice, the mean wavelength of the laser source is positioned on the center of the absorption line of the analyzed gas by adjusting the laser DC current and the temperature of the laser chip.

Typically, the temperature adjustment slope is 0.1–0.2 nm/K. The fast wavelength modulation is accomplished by adding a sinusoidal small-amplitude current at the frequency f to the DC driving current of the laser. The current tuning factor is 0.01–0.02 nm/mA. The modulation current is adjusted to make the laser output line sweep back and forth across the absorption line of the gas. The photoacoustic signal is generated by the line absorption at the frequency $2f$ but the photoacoustic background signal from windows, walls of the sample cell, and the cantilever itself appears at the frequency f; thus, it is possible to eliminate background effects by picking only the signal at $2f$.

Secondly, the sample cell should be designed for the laser source; i.e., the diameter should be so small that the laser beam fills it as well as possible. This maximizes the response in the gas and guarantees the best performance of the system.

The first study with a cantilever microphone and tunable laser source was realized using non-optimal sample cell structure (24, 25) for CO_2 gas concentration measurements. The diameter of the cells was 10 mm and the volume 8 cm^3. The laser beam was collimated with a fiber collimator and fed to the cell through a calcium window. The laser beam reflected from the silver-coated cantilever and thus travelled twice the sample cell. The wavelength of the telecommunication laser was 1572 nm and the output power about 50 mW. Around this wavelength there are three rotational absorption lines of CO_2. None of these lines is very strong, but they were selected because a suitable telecommunication laser is available. When using the strongest line at the total pressure of 250 mbar, the minimum detectable CO_2 mole fraction was 7.2 ppm with the measurements time of 110 s. The detection limit was estimated from the noise level of the system ($SNR = 1$).

Slightly better results were observed with another sample cell structure (26, 27). The cell diameter was 3 mm and the length 40 mm; the total volume including the small buffer was 1.7 cm^3. The laser source was the same as in a previous study (24, 25). With the output power of 34 mW, the detection limit for CO_2 was 4.0 ppm. The output power of the diode laser can be increased by amplifying the laser light with an ytterbium-erbium co-doped fiber amplifier. The nominal maximal output power was 1 W, but in practice the maximal power transmitted through the cell was 650–700 mW. At the power of 600 mW, the detection limit for CO_2 was 0.23 ppm. These figures can be used to estimate the detection limit of other gases by utilizing the data of their line strengths. At the power of 30 mW, the corresponding limits are 69 ppb for CH_4, 33 ppb for NH_3, and 3.6 ppm for CO. In this study it was also observed that the photoacoustic response depends on the solvent gas: when using similar CO_2 concentrations, the photoacoustic signal was 60% lower in nitrogen than in argon.

The similar cell structure (length 61 mm, diameter 3 mm) has been used for sensitive oxygen detection (28). As a light source, a tunable DFB diode

laser (output power 30 mW) and a VCSEL (vertical-cavity surface-emitting; output power 0.5 mW) laser were used, both operating near 760 nm. Unfortunately, the only absorption band of oxygen within the spectral range covered by diode lasers is a weak magnetic dipole transition at this wavelength, and therefore low detection limits are difficult to achieve. However, the high sensitivity of photoacoustic method with a cantilever-enhanced technique can provide a potential alternative over traditional absorption methods. The noise-equivalent detection limits for oxygen were 20 ppm with the DFB laser and 500 ppm with the VCSEL when the measurement time was 68 s, corresponding to average of 100 individual FFT spectra. These figures point out that for practical demands in oxygen sensors, for example, in biomedicine, the demonstrated sensitivity is sufficient. Some VCSEL lasers can also operate at significantly longer wavelengths where stronger absorption lines of many interesting gases exist, and thus much higher sensitivities can be expected. However, currently, such VCSELs have very low output power or they must be operated at cryogenic temperatures, and they are also very expensive. In the future we can assume that the manufacturing technology of VCSELs will further develop when they are very promising components for photoacoustic applications.

Currently, the best result when using cantilever-enhanced photoacoustic method with laser source is the detection limit of 0.33 ppm for CO_2 (29). The output power of the DFB laser was 30 mW and the measurement time 100 s. The achieved normalized noise equivalent sensitivity of $1.7 \times 10^{-10}\text{cm}^{-1}\ \text{W}/\sqrt{\text{Hz}}$ is the best ever reported with laser-based photoacoustic trace gas detectors. The improvement of the detection limit was achieved by optimizing the cell size and structure, cantilever dimensions, and the interferometer measurement system. However, there are still possibilities to further improve the performance by optimizing the total pressure in the photoacoustic cell together with the depth and the symmetry of the laser wavelength modulation.

Lindley et al. (30) made comparisons between different photoacoustic cell structures and microphones. In the first setup they used a hollow 80-mm stainless steel tube, which acted as an acoustic resonator; the resonance frequency was 2 kHz. The microphone was a conventional electret capacitor microphone. The light source was a diode laser operating at a wavelength of 1530 nm and output power of 30 mW. The wavelength was selected to match the combined rotational-vibrational line of acetylene. The second cell configuration consisted of two cylindrical acoustic resonator flow tubes that were 5.5 mm in diameter. Both tubes housed a microphone but the laser radiation was directed through only one to generate the photoacoustic signal. The resonance frequency of the tubes was 4 kHz. By subtracting the signal of the reference cell from the one of the photoacoustic cells would remove any noise components that are coherent in both resonators. The third cell design contained a cantilever pressure sensor attached to the 115-mm cylindrical copper tube with a diameter of 3 mm. This configuration

was used well below the acoustic resonance frequency of the cell and the mechanical resonance of the cantilever. The same laser source was used in all three cell designs but the modulation scheme was different: for the first and second systems, the amplitude of the laser output was modulated at the resonance frequency of the acoustical resonator, but in the case of the cantilever microphone, the wavelength of the light was modulated. The results from these three different setups clearly demonstrated that the cantilever-based microphone in the non-resonator cell was the most sensitive for trace gas measurements. In fact, the cantilever microphone was 100 times better than either the differential or single-microphone cells. Superior performance of the cantilever cell demonstrates that it is less vulnerable to residual ambient noise under conditions where traditional microphone cell performances are compromised.

Cantilever Microphone in FTIR Applications

Low-resolution Fourier-transform infrared (FTIR) spectrometers are the best instruments for trace gas analysis when a broadband black-body radiation source and a normal absorption technique is used. Currently, modern FTIR gas analyzers are already working very close to their theoretical limits and thus the only possibility to improve their performance is to use new technology. Photoacoustic sensors are seldom used in gas-phase FTIR, but their benefits have been demonstrated in solid-phase FTIR spectroscopy. Photoacoustic detectors based on conventional condenser microphones normally do not have such a high sensitivity as needed for FTIR applications. It is possible to enhance the sensitivity using acoustical resonances of the sample cell, but such devices are not useful for FTIR purposes because FTIR systems require a wide frequency band. However, the cantilever pressure sensor has a sensitivity even several orders higher than the conventional microphones, and the frequency band is wide.

Typical conventional gas-phase FTIR spectrometers consist of a large White multipass cell of few liters in volume and very expensive mirrors. They also severely suffer nonlinearities due to Beer's law because the absorption path length can be several meters. This can be a very serious limitation when analyzing wet gases due to strong water absorption over a wide wavelength range. With cantilever-based microphones, the cell can be very small in volume and the absorption path length only few millimeters, which practically cancels all nonlinearities and water problems.

The example spectrum of methane of 100 ppm in nitrogen from the first preliminary study with a cantilever microphone in FTIR spectrometer is presented in Figure 4. The original detector in the commercial FTIR system was replaced with the photoacoustic cell for measurements. The broadband spectrum of methane compares very well with one obtained by using the conventional detector.

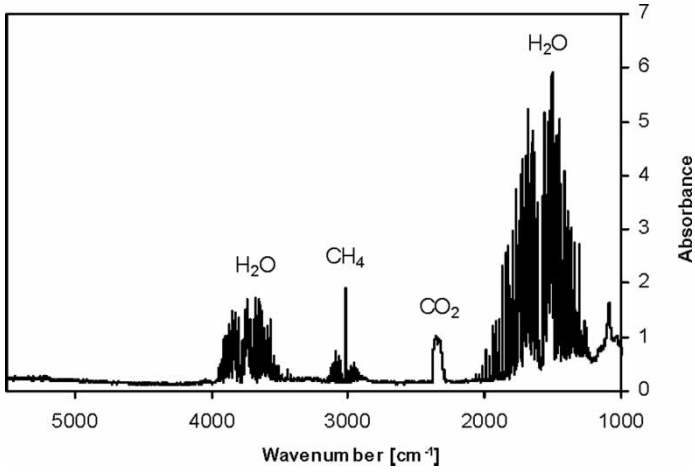

Figure 4. The photoacoustic FTIR spectrum of 100 ppm of methane (CH_4) in nitrogen (the total pressure 1 atm) measured with the cantilever-based microphone. The other absorption bands are due to the water (H_2O) and carbon dioxide (CO_2) impurities.

OTHER CONSTRUCTIONS

Double Cantilever System

Acceleration and acoustical noises can be minimized in the simplest photoacoustic designs only by using acoustic isolators and vibration dampers of the sample cell. In practice, it can be very difficult to prevent, especially low-frequency acceleration noise produced by the environment. One solution is to use the double cantilever design. In this construction, there are two interferometric cantilever microphones installed on the opposite sides of the sample cell facing each other. The photoacoustic effect produces, as usual, a signal on both microphones, but the phase difference of those signals is 180 degrees; i.e., the cantilevers bend to opposite directions. In contrast, the acceleration of the whole system, in the perpendicular direction to the plane of the cantilevers, also generates signals on both microphones but now the phase difference is zero. The acceleration part of the signal can be eliminated simply by subtracting the two signals of the microphones. This method is highly sensitive to the phase errors of the signals, but even if the phases are not absolutely correct, the acceleration noise can be substantially decreased, even on the order of thousands.

Balance Chamber Designs

The acceleration noise is generated not only from the acceleration of the cantilever itself due to its inertia but also the acceleration of the gas inside

the sample cell. These can be eliminated or at least decreased using the double cantilever system, but there is also another, much simpler, method to decrease these kinds of disturbances.

The acceleration affects the pressure inside the sample cell and the interferometer chamber linearly

$$p = p_0 - \rho_{gas} a x \tag{62}$$

where p_0 is the original pressure of the cell, ρ_{gas} the density of the gas, a the acceleration, and x the coordinate along the cell in the direction of the acceleration. The pressures in the sample cell and the interferometer chamber are shown in Figure 5. Exactly at the position of the center of the mass of the gas in the cell or chamber, the pressure does not encounter any changes due to the acceleration, but in other parts it changes linearly according to Eq. (62). The effective (differential) pressure on the cantilever is then given by

$$p_{eff} = \frac{m_{cant}}{A} + \rho_{gas} D_c a = \rho_{cant} d a + \rho_{gas} D_c a \tag{63}$$

where m_{cant} is the mass, ρ_{cant} the density, A the area, and d the thickness of the cantilever, and D_c the distance of the center of the gas mass of the chambers. The first term in Eq. (63) is "pressure" due to inertia of the cantilever and the second term because of the movement of the gas. Normally these two components affect the same direction and increase the effect of the acceleration noise. It should be noted that only the distance between the center of the mass is important, not the detailed structure of the chambers.

If another chamber, a so-called balance chamber, is added to the system as described in Figure 6, it is possible to cancel both acceleration terms in Eq. (63). This additional chamber is connected to the left chamber and therefore

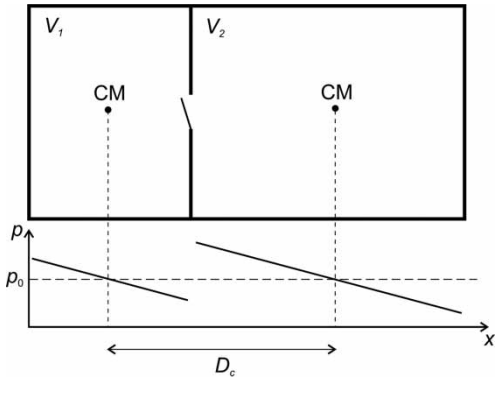

Figure 5. The pressure changes in the gas chambers due to external acceleration of the device. The center of the mass of the gas in both chambers is labeled "CM."

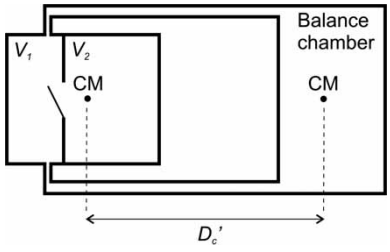

Figure 6. The structure of the damping system for acceleration noise consisting of the special balance chamber.

it generates opposite pressure on the cantilever under acceleration on that chambers. Now we obtain the effective pressure p_{eff}

$$p_{eff} = \rho_{cant} da + \rho_{gas}(-D_c')a \tag{64}$$

where D_c' is the distance between the combined position of the center of mass of the sample cell and the interferometer chamber and the one of the balance chamber. We can adjust $p_{eff} = 0$ if we set

$$D_c' = \frac{\rho_{cant}}{\rho_{gas}} d \tag{65}$$

In practical implementations, the distance D_c' can be adjusted by changing the volume or shape of the balance chamber. This construction eliminates acceleration noise due to the inertia of the cantilever and the gas in the direction of the acceleration component perpendicular to the cantilever surface. In the directions parallel to the cantilever surface, we do not have any cantilever inertia, and then the noise can be eliminated by positioning the cantilever to position of the center of mass in those directions.

The efficiency of the balance chamber method depends on the frequency of the acceleration noise. In the low-frequency range, the damping factor goes to zero since the pressure difference over the cantilever gradually vanishes because of the leak of the gas between the cantilever and its frame. This cut-on frequency is determined by the characteristic time constant (32). In the high-frequency range, the damping factor also decreases because of the slowness of the gas to achieve the linear pressure dependence (62); this time constant is related to the speed of sound. In theory, the damping factor is infinite at a certain frequency, but in practice in the middle frequencies a damping factor as high as 400 has been measured.

Differential System

In the long path absorption spectroscopy, the light beam penetrates through the sample gas, and the absorption at two or more wavelengths is measured

and compared. The sensitivity of this method depends mainly on the absorption length, output power of the light source, and response of the detector. In practice, the absorption path length cannot be increased too much since, because of the exponential decreasing of the signal, the signal-to-noise ratio would be very small, and with wet gases the water absorption can be serious problem.

In differential photoacoustic detection, the selectivity of the traditional absorption method and the high sensitivity of the detector are combined. The basic structure of this system is shown in Figure 7. The device consists of three cells: the sample cell containing the unknown concentration of the gas to be detected, the reference cell filled with pure nitrogen, and the differential photoacoustic cell containing a high concentration of the analyzed gas. The differential cell is divided into two equal parts and the cantilever is between them; the bending of the cantilever is measured by using the interferometer (not shown in Figure 7). If there is a pressure difference over the cantilever, it bends proportionally to that difference; i.e., it acts like a highly sensitive differential pressure sensor. The infrared radiation is directed to the sample and reference cell with an equal power. From these cells the radiation enters to the both parts of the differential cell.

The pressure difference can be generated only if the light absorption is different on both sides of the cantilever, and this is possible only if there has been some absorption of light in the sample cell at the same wavelength specific to the analyzed gas. Thus, the pressure difference and the bending of the cantilever are directly related to the concentration of the gas.

The first experiments using the differential phototoacoustic method have demonstrated that this approach can be highly selective (31). The essential advantage of this method is that there is no need to use complex filter banks since the gas itself acts as a filter. It is also possible to use a mixture of

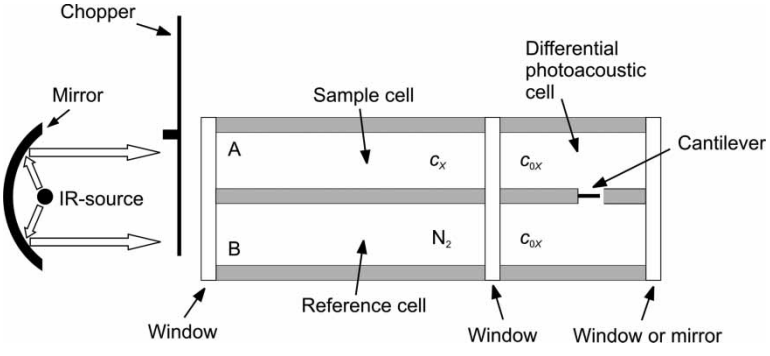

Figure 7. Construction of the differential photoacoustic system. The sample cell A contains unknown concentration c_X of the gas to be detected, the reference cell B is filled with pure nitrogen, and the differential photoacoustic cell contains a high concentration c_{0X} of the analyzed gas.

gases in the differential cell and perform multicomponent analysis of trace gases. Since the sample cell is not part of the photoacoustic cell, open-air measurements can also be done without remarkable interference of the ambient noise.

PRACTICAL IMPLEMENTATION

The real construction of the photoacoustic system is somewhat different than the principal schema, as shown in Figure 8. The sample cell is a long tube and the cantilever (not visible in the figure) is positioned at the end of the narrow side tube attached at the middle of the sample tube. The interferometer itself is not closed into the chamber, but that volume is kept as small as possible. The small compartment on the other side of the cantilever is closed with the beam splitter, which is actually a small quartz cube. The laser beam is directed downwards to the cantilever. Detector photodiodes are directly glued on the faces of the beam splitter. The balance chamber is also a tube positioned parallel to the sample cell. The overall dimensions of the device are

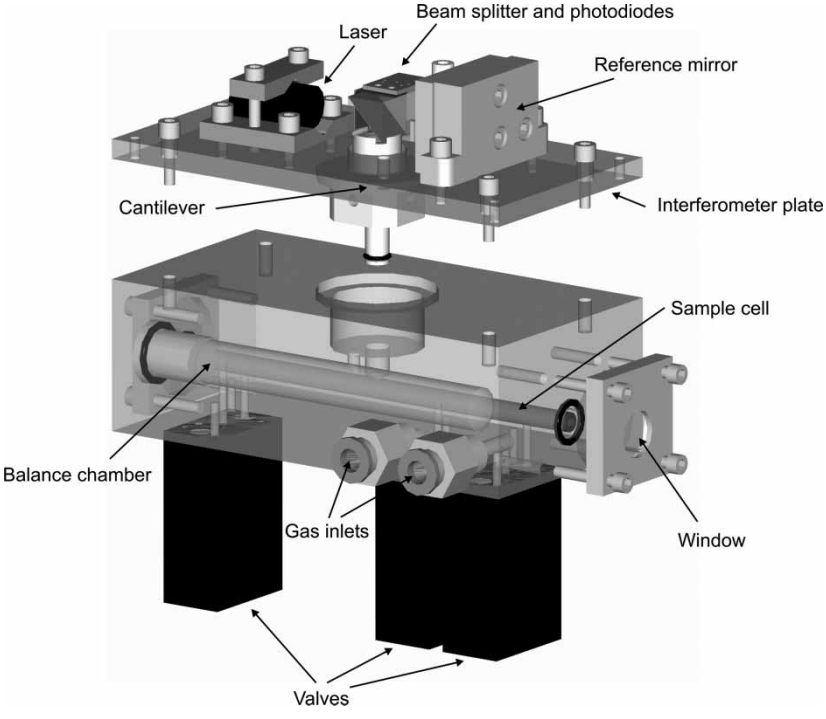

Figure 8. The realistic structure of the photoacoustic cell with the cantilever and the interferometer manufactured by Gasera Ltd (Turku, Finland).

$120 \times 120 \times 60\ mm^3$. Three valves are used to purge, flush, and fill the sample tube. This construction has been used in the experiments reported in Koskinen et al. (29).

REFERENCES

1. Bell, A.G. (1881) Upon the production of sound by radiant energy. *Philosophical Magazine J. Sci.*, 11: 510–528.
2. Tyndall, J. (1881) Action of an intermittent beam of radiant heat upon gaseous matter. *Proceedings of the Royal Society*, 31: 307–317.
3. Kerr, E.L. and Atwood, J.G. (1968) The laser illuminated absorptivity spectrophone: A method for measurement of weak absorptivity in gases at laser wavelengths. *Applied Optics*, 7: 915–921.
4. Kreuzer, L.B. (1971) Ultralow gas concentration infrared absorption spectroscopy. *Journal of Applied Physics*, 42: 2934–2943.
5. West, G.A., Barret, J.J., Siebert, D.R., and Reddy, K.V. (1983) Photoacoustic spectroscopy. *Review of Scientific Instruments*, 54: 797–817.
6. Miklos, A. and Hess, P. (2001) Application of acoustic resonators in photoacoustic trace gas analysis and metrology. *Review of Scientific Instruments*, 72: 1937–1955.
7. Wilcken, K. and Kauppinen, J. (2003) Optimization of a microphone for photoacoustic spectroscopy. *Applied Spectroscopy*, 57: 1087–1092.
8. Kauppinen, J., Wilcken, K., Kauppinen, I., and Koskinen, V. (2004) High sensitivity in gas analysis with photoacoustic detection. *Microchemical Journal*, 76: 151–159.
9. Koskinen, V., Fonsen, J., Kauppinen, J., and Kauppinen, I. (2006) Extremely sensitive trace gas analysis with modern photoacoustic spectroscopy. *Vibrational Spectroscopy*, 42: 239–242.
10. de Paula, M.H., de Carvalho, A.A., Vinha, C.A., Cella, N., and Vargas, H. (1988) Optical microphone for photoacoustic spectroscopy. *Journal of Applied Physics*, 64: 3722–3724.
11. Park, S.M. and Diebold, G.J. (1987) Interferometric microphone for photoacoustic spectroscopy. *Review of Scientific Instruments*, 58: 772–775.
12. Kosterev, A.A., Bakhirkin, Yu.A., Curl, R.F., and Tittel, F.K. (2002) Quartz-enhanced photoacoustic spectroscopy. *Optics Letters*, 27: 1902–1904.
13. Kosterev, A.A., Bakhirkin, Y.A., and Tittel, F.K. (2005) Ultrasensitive gas detection by quartz-enhanced photoacoustic spectroscopy in the fundamental molecular absorption bands region. *Applied Physics B*, 80: 133–138.
14. Rabe, U., Janser, K., and Arnold, W. (1996) Vibrations of free and surface-coupled atomic force microscope cantilevers: Theory and experiment. *Review of Scientific Instruments*, 67: 3281–3293.
15. Carslaw, H.S. and Jaeger, J.C. (1959) *Conduction of Heat in Solids*; Oxford University Press: London.
16. Gittes, F. and Schmidt, C.F. (1998) Thermal noise limitations of micromechanical experiments. *European Biophysics Journal*, 27: 75–81.
17. Salapaka, M.V., Berg, H.S., Lai, J., Majumdar, A., and McFarland, E. (1997) Multi-mode noise analysis of cantilevers for scanning probe microscopy. *Journal of Applied Physics*, 81: 2480–2487.
18. Saulson, P.R. (1990) Thermal noise in mechanical experiments. *Physical Review D*, 42: 2437–2445.

19. Callen, H.B. and Greene, R.F. (1952) On a theorem of irreversible thermodynamics. *Physical Review*, 86: 702–710.
20. Bruland, K.J., Garbini, J.L., and Dougherty, W.M. (1996) Optimal control of force microscope cantilevers. II. Magnetic coupling implementation. *Journal of Applied Physics*, 80: 1959–1964.
21. Garbini, J.L., Bruland, K.J., and Dougherty, W.M. (1996) Optimal control of force microscope cantilevers. I. Control design. *Journal of Applied Physics*, 80: 1951–1958.
22. Liang, S., Medich, D., Czajkowsky, D.M., Sheng, S., Yuan, J.-Y., and Shao, Z. (2000) Thermal noise reduction of mechanical oscillators by actively controlled external dissipative forces. *Ultramicroscopy*, 84: 119–125.
23. Tamayo, J. (2005) Study of the noise of micromechanical oscillators under quality factor enchancement via driving force control. *Journal of Applied Physics*, 97: 044903-1-10.
24. Laurila, T., Cattaneo, H., Koskinen, V., and Kauppinen, J. (2005) Diode laser-based photoacoustic spectroscopy with interferometrically-enhanced cantilever detection. *Optics Express*, 13: 2453–2458.
25. Laurila, T., Cattaneo, H., Koskinen, V., and Kauppinen, J. (2005) Diode laser-based photoacoustic spectroscopy with interferometrically-enhanced cantilever detection: Erratum. *Optics Express*, 14: 4195–4195.
26. Laurila, T., Cattaneo, H., Pöyhönen, T., Koskinen, V., Kauppinen, J., and Hernberg, R. (2006) Cantilever-based photoacoustic detection of carbon dioxide using a fiber-amplified diode laser. *Applied Physics B*, 83: 285–288.
27. Laurila, T., Cattaneo, H., Pöyhönen, T., Koskinen, V., Kauppinen, J., and Hernberg, R. (2006) Cantilever-based photoacoustic detection of carbon dioxide using a fiber-amplified diode laser. Erratum. *Applied Physics B*, 83: 669.
28. Cattaneo, H., Laurila, T., and Hernberg, R. (2006) Photoacoustic detection of oxygen using cantilever enhanced technique. *Applied Physics B*, 85: 337–341.
29. Koskinen, V., Fonsen, J., Rorh, K., and Kauppinen, J. (2007) cantilever enhanced photoacoustic detection of carbon dioxide using a tunable diode laser source. *Applied Physics B*, 86: 451–454.
30. Lindley, R.E., Parkes, A.M., Keen, K.A., McNaghten, E.D., and Orr-Ewing, A.J. (2007) A sensitive comparison of three photoacoustic cells containing a single microphone, a differential dual microphone or a cantilever pressure sensor. *Applied Physics B*, 86: 707–713.
31. Uotila, J., Koskinen, V., and Kauppinen, J. (2005) Selective differential photoacoustic method for trace gas analysis. *Vibrational Spectroscopy*, 38: 3–9.